Journal of Theoretical and Computational Acoustics
Vol. 29, No. 4 (2021) 2150025 (22 pages)

DOI: 10.1142/S2591728521500250

Partition of Unity Finite Element Method for 2D Vibro-Acoustic Modeling

Christophe Langlois*, Jean-Daniel Chazot*,‡, Li Cheng†
and Emmanuel Perrey-Debain*

*Roberval (Mechanics, Energy and Electricity)
Centre de Recherche Royallieu
Université de Technologie de Compiègne
CS 60319, 60203 Compiègne Cedex, France

†Department of Mechanical Engineering
The Hong Kong Polytechnic University
Hong Kong, P. R. China

‡jean-daniel.chazot@utc.fr

Received 16 June 2021
Accepted 9 November 2021
Published 27 December 2021

The Partition of Unity Finite Element Method (PUFEM) shows promise for modeling wave-like problems in the mid-to-high frequency range, allowing to capture several wavelengths in a single element. Despite the increasing attention it received in acoustics and in structural dynamics, its efficacy to deal with coupled problems has not been addressed. The main challenge in this case is to be able to represent different types of physical waves accurately, knowing that the wavelengths can be very different and vary differently, exemplified by the dispersion of flexural waves in a solid. Without a proper handling of the coupling between the coupled media, at best the number of degrees of freedom (DoF) will not be optimal, at worst the coupled model will not converge. Techniques like mesh refinement, wave enrichment and compatible or incompatible meshes might offer a potential solution to the problem, but the model usually needs to be adjusted through a time consuming trial-and-error procedure. To tackle the problem, this paper considers a 2D coupled vibro-acoustic problem, in which the structural and acoustic domains, modeled with PUFEM, are coupled using compatible and incompatible meshes based on different coupling strategies. Numerical analyses show that the proposed method outperforms the classical finite element method by several orders of magnitude in terms of number of DoF. Recommendations are proposed on the technique to choose depending on the frequency range of interest in relation to the critical frequency of the structure to ensure the best convergence rate. Finally, an application example is presented to highlight the performance of the proposed method.

Keywords: PUFEM; vibro-acoustic; coupling; fluid-structure; mid to high frequency.

‡Corresponding author.

1. Introduction

Vibro-acoustic problems are challenging to solve and have received a lot of attention over the past decades. The two most commonly used methods to solve such problems are the finite element method (FEM)[1] and the boundary element method (BEM).[2] On the one hand, FEM uses domain discretization and describes the problem with sparsely populated matrices. On the other hand, with BEM, only the boundary is discretized, leading to fully populated matrices. These two methods are robust and commonly used in the industrial and scientific world to solve a wide range of problems. However, their efficiency is significantly compromised in the so-called mid-to-high frequency range when the number of wavelengths in the domain can be overwhelmingly large. Indeed, to reach a decent level of accuracy, the number of degrees of freedom (DoF) has to be increased. This leads to very large matrices which increase tremendously the computational cost. In addition, with classical FEM, as the level of discretization increases, dispersion error and pollution problem would also arise.[3–5]

Several methods have been developed to cope with the specific need of higher frequency range problems at a reasonable cost. The statistical energy analysis (SEA) is conventionally used to reach the high-frequency range. The hybrid determinist-statistical method, born in the 90s[6,7] is another alternative that still receives attention nowadays.[8] With this method, the domain with small wave numbers (large wavelengths) can be modeled by FEM and the other one with large wave numbers by SEA. The main issue with this hybrid method is that the results obtained are not deterministic and the wave field domain cannot be recovered. In addition, this method can only be suited to a frequency range which meets SEA requirements, in other words the method is bound to model diffuse fields only.

The mid-to-high frequency range, outside the SEA application scope, is a range in which wave fields can still and need to be described accurately. The particular study of guided waves and periodic domains led to the Wave Finite Element Method (Wave-FEM).[9] For less specific problems, a popular trend to reach this frequency range is to include information of the basic wave solutions into the classical FEM framework as enrichment. Such effort led to the wave envelope approach,[10] the discontinuous Galerkin method,[11–13] the Trefftz-based approach,[14] the wave-based method (WBM),[15] the variational theory of complex rays (VTCR),[16] etc. For an in-depth literature review on existing approaches, see Ref. 17.

Another method used to model wave-like problems is the Partition of Unity FEM (PUFEM).[18,19] The method has been first developed to solve acoustic problems. It is a mesh-based method in which a function basis is added at the nodes of the discretized elements. By doing so, elements span over several wavelengths while maintaining the precision of the model. The method has received intensive attention in acoustics. Typical efforts include the development of accurate models by using plane waves which are solution to the homogeneous Helmholtz equation as function basis[20]; efficiency improvement using exact integration schemes in two dimensions[21] and in three dimensions[22]; modeling of the sound absorbing and poroelastic media[23,24]; the modeling of nonreflecting boundary conditions (NRBCs),[25,26] etc. On the structural side, the PUFEM has also been attempted in modeling vibrations of 1D Timoshenko[27] and Euler–Bernoulli beams.[28] Meanwhile, PUFEM

has also been applied to solve 2D elastodynamic problems[29] and specific thin plates problems.[30] For the former, efforts have also been made to reduce the CPU time by designing exact integration schemes.[31] Finally, given its ability to capture small and spatially varying wavelength oscillations, PUFEM has been used to model 1D acoustic black hole (ABH) structures.[32] More recently, partition of unity has been studied in an isogeometric framework leading to the so-called Partition of Unity Isogeometric Analysis (PUIGA) which enhances the efficiency of the partition of unity when the geometry of the domain is complex.[33,34] The strength of the method being its ability to model highly oscillatory wave fields at low computational cost, it was naturally used and further developed in other fields of physics, for example, in electromagnetics.[35]

In contrast with other methods suited for the mid-to-high frequency range, the PUFEM does not need the exact solution of the wave equation, which makes it a very flexible method. In addition, contrary to the WBM for example, it is not limited to solely convex geometries. Finally, since it is an extension of the classical FEM, it is fairly easy to be implemented and incorporated into an existing FEM framework. Surprisingly, PUFEM has received little attention in dealing with fluid–structure interaction problems. Related effort includes its embodiment into the improved element-free Galerkin method (I-EFGM),[36,37] in which a 2D structural domain is modeled using PUFEM before being coupled to an acoustic domain modeled using I-EFGM. To the best of authors' knowledge, exploration on the use of PUFEM to model both the structural and acoustic domains in a fluid–structure interaction problem has not been reported in the open literature. Yet these problems are technically challenging from numerical perspective. Indeed, due to the differences in wave propagation properties in solid and acoustic medium, each domain bears different wavelengths with different variation trends with respect to frequency. The PUFEM requirements for good convergence are therefore also different for the two domains, each requiring a different level of discretization. As a result, how to conciliate different and sometimes competing factors involved in the PUFEM modeling becomes an important question. In addition, evanescent waves are also radiated in the acoustic domain below the critical frequency of the structure, in the vicinity of the coupling interface. The presence of both propagating and evanescent waves can possibly deteriorate the performances of the method and must be carefully handled.

In this paper, a general 2D fluid–structure coupling problem is investigated, in which both acoustic and structural domains are modeled using PUFEM. Considering the differences in the wavelengths of the two media and their respective variation trends with respect to frequency, two coupling strategies are investigated: compatible meshes and incompatible meshes. In Sec. 2.1, the general coupling problem is formulated. Governing equations are developed for each domain along with the coupling equations. In Secs. 2.2 and 2.3, the variational equations and PUFEM formulation of both domains are given. Coupling strategies are explained in Sec. 2.4. In Sec. 3, the proposed coupling strategies are tested and compared with standard FEM. Finally in Sec. 4, the method is applied to model a vessel submerged in water as a real-life problem involving strong vibro-acoustic coupling.

2. Formulation

2.1. *Problem statement*

Without limiting the generality of the method, the mathematical formulation of the vibro-acoustic problem is presented here for the case of a simple configuration illustrated in Fig. 1. The bi-dimensional acoustic domain Ω_f is filled with a fluid at rest with density ρ_f and speed of sound c_f. Its boundary is regrouped into two sub-boundaries $\partial\Omega_f = \Gamma_f \cup \Gamma_s$ where Γ_s corresponds to the interface with a 1D vibrating structure, here a beam, for which specific fluid–structure coupling conditions are to be prescribed, whereas Γ_f refers to the remaining part of the boundary where classical conditions, i.e. rigid wall, impedance wall and/or radiation conditions, are applied. The coordinate system (x, y, z), also shown in the figure, is defined to ensure that the vibrating structure is aligned with the coordinate x. In the acoustic domain, the pressure p obeys the Helmholtz equation:

$$\Delta p + k_f^2 p = 0 \quad \text{in } \Omega_f, \tag{1}$$

where $\Delta = \boldsymbol{\nabla}^2$ is the Laplace operator and $k_f = \omega/c_f$ is the acoustic wave number. Here, ω is the angular frequency and the time convention used throughout this paper is $\mathrm{e}^{-\mathrm{i}\omega t}$, with $\mathrm{i}^2 = -1$. On the boundary Γ_f, the general Robin-type condition is applied and

$$\partial_n p = Bp + g, \tag{2}$$

where B is boundary operator (which is not necessarily local) and g stands for a source term which is proportional to a prescribed velocity. The vibrating beam considered in this work is assumed to be thin, uniform and pinned at both ends. Its vibration is described by its transverse displacement w, governed by the Euler–Bernoulli theory as

$$EI\frac{\partial^4 w}{\partial x^4} - \omega^2 \rho_s S w = Q, \tag{3}$$

where E is Young's modulus; $I = bd^3/12$ is the second moment of area; b is the width of the beam; d its thickness; ρ_s its density and $S = bd$ its cross-section area. Q is the total load acting on the beam Γ_s which also comprises the fluid loading and an external

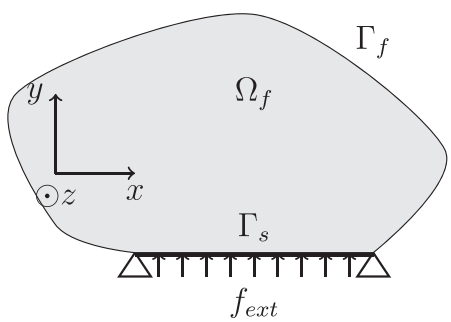

Fig. 1. General coupling case.

excitation f_{ext}, i.e.

$$Q = f_{\text{ext}} - pb. \tag{4}$$

The coupling between the fluid domain and the beam is ensured by imposing the continuity of displacement:

$$\frac{1}{\rho_f \omega^2} \frac{\partial p}{\partial n} = w, \tag{5}$$

where n is the unit normal pointing outward. The left-hand side of Eq. (5) represents the acoustic displacement along the positive y-direction.

2.2. *Variational formulations*

The derivation of the corresponding variational formulation for both the acoustic domain and the vibrating structure is straightforward and well known, which is recalled here for completeness. The Helmholtz equation is transformed using standard weighted residual scheme as

$$\int_{\Omega_f} (\nabla p \nabla \delta p - k_f^2 p \delta p) \mathrm{d}\Omega = \int_{\partial\Omega_f} \delta p \partial_n p \mathrm{d}\Gamma, \tag{6}$$

where δp denotes the weighting function. Similarly, the variational formulation for the beam writes

$$\int_{\Gamma_s} \left(EI \frac{\partial^2 w}{\partial x^2} \frac{\partial^2 \delta w}{\partial x^2} - \omega^2 \rho_s S w \delta w \right) \mathrm{d}\Gamma = \int_{\Gamma_s} \delta w Q \mathrm{d}\Gamma + \delta w(0)\lambda_0 + \delta w(L)\lambda_L, \tag{7}$$

where δw is the weighting function and λ_0 and λ_L are Lagrange multipliers used to impose the pinned boundary condition at both ends of the beam (at $x = 0$ and $x = L$) (for more details refer to Ref. 28). Combining the coupling equations (5) and (4) with Eqs. (6) and (7), respectively, leads to the following coupled system of equations:

$$\int_{\Omega_f} \nabla p \nabla \delta p \mathrm{d}\Omega - k_f^2 \int_{\Omega_f} p \delta p \mathrm{d}\Omega - \int_{\Gamma_f} B p \delta p \mathrm{d}\Gamma - \rho_f \omega^2 \int_{\Gamma_s} w \delta p \mathrm{d}\Gamma = \int_{\Gamma_f} g \delta p \mathrm{d}\Gamma, \tag{8}$$

$$EI \int_{\Gamma_s} \frac{\partial^2 w}{\partial x^2} \frac{\partial^2 \delta w}{\partial x^2} \mathrm{d}\Gamma - \omega^2 \rho_s S \int_{\Gamma_s} w \delta w \mathrm{d}\Gamma + \int_{\Gamma_s} \delta w p b \mathrm{d}\Gamma - \delta w(0)\lambda_0 - \delta w(L)\lambda_L = \int_{\Gamma_s} \delta w f_{\text{ext}} \mathrm{d}\Gamma. \tag{9}$$

Coping with different types of variables, pressure and displacement in this case, may introduce numerical issues such as ill-conditioned matrices. To avoid this, pressure terms are scaled to be homogeneous to a displacement. As a result, instead of solving for (p, w), the model is solved for $(p/(\rho_f c_f \omega), w)$. If there are several fluid domains (i.e. if both sides of the structure are wet) then the change of variable is performed for each acoustic domain using its respective physical properties.

2.3. *PUFEM formulations*

PUFEM is built on classical FEM meshes and its key ingredient relies on the enrichment of the finite element solution space by including more specific functions in order to better capture the oscillating behavior of the solution. The acoustic domain Ω_f is partitioned into nonoverlapping elements where each element is defined via a mapping relationship function $\mathbf{r}(\xi, \eta)$ between the real space and the local system of triangular type. Because PUFEM elements are expected to span over many acoustic wavelengths, the mapping should describe the geometry of the boundary with sufficient accuracy. In this work, a quadratic mapping using T6 elements is used as in Ref. 24, knowing that high-order approximations can be easily implemented. The pressure in each element is approximated using classical plane wave enrichment function as

$$p(\mathbf{r}(\xi,\eta)) = \sum_{j=1}^{3} \sum_{q=1}^{\mathcal{Q}_j} N_j(\xi,\eta) \exp(\mathrm{i}k_f(\mathbf{r}(\xi,\eta) - \mathbf{r}_j) \cdot \mathbf{d}_{jq}) A_{jq}, \tag{10}$$

where function N_j is the classical linear shape functions for a triangular element, $\mathbf{r}_j$ is the position vector of node j, $\mathcal{Q}_j$ the number of plane waves attached to node j and the A_{jq}'s are unknown plane wave coefficients. Propagation directions are chosen to be evenly spaced and

$$\mathbf{d}_{jq} = \begin{pmatrix} \cos\alpha_{jq} \\ \sin\alpha_{jq} \end{pmatrix} \quad \text{where } \alpha_{jq} = q\frac{2\pi}{\mathcal{Q}_j}. \tag{11}$$

Criteria are provided in Ref. 38 to determine the necessary number of plane waves at each node of the mesh. This number solely depends on the size of the element with respect to the acoustic wavelength and

$$\mathcal{Q}_j = \mathrm{round}(k_f h_f + C(k_f h_f)^{1/3}), \tag{12}$$

where h_f is the longest acoustic element edge attached to node j and C is an integer chosen in the interval $[2, 20]$. This parameter C can be used to increase the level of discretization of the numerical model.

Depending on the shape of the element, two integration schemes are considered. As mentioned previously, the geometry is quadratically mapped on T6 elements. When a T6 has straight edges, it can be considered as a T3 element, in which case element matrices are computed using an exact integration scheme as described in Ref. 22. If at least one edge of the T6 element is curved, then the Gauss–Legendre quadrature is used in which case integration points and their associated weights are obtained via a Cartesian product as described in Ref. 39.

The vibrating structure Γ_s is partitioned into $m = 1 \ldots M$ linear elements $\Gamma_s^m = \{x(\mu), \mu \in [-1, 1]\}$ and the transverse displacement w in each element is expressed using the following PUFEM approximation[28]:

$$w(x) = \sum_{i=1}^{2} \sum_{k=1}^{6} N_i^h(\mu) \Psi_{ik}(x) W_{ik}, \tag{13}$$

where N_i^h represent the classical 1D Hermitian shape functions defined on the interval $[-1, 1]$

$$N_1^h(\mu) = \frac{(1-\mu)^2(2+\mu)}{4} \quad \text{and} \quad N_2^h = \frac{(1+\mu)^2(2-\mu)}{4}. \tag{14}$$

Using Hermitian shape functions is necessary to ensure inter-element C^1 continuity. In Eq. (13), the basis enrichment functions are constructed using a combination of low-order polynomials and propagating waves which are solution of the *in vacuo* homogeneous problem, namely

$$\Psi_{ik} = \{1, \tilde{x}_i, \tilde{x}_i^2, \tilde{x}_i^3, \cos(k_s\tilde{x}_i), \sin(k_s\tilde{x}_i)\}, \tag{15}$$

with $\tilde{x}_i = x - x_i$ where x_i is the coordinate of node i and k_s is the *in vacuo* flexural wave number given by

$$k_s = \sqrt[4]{\frac{\rho_s S\omega^2}{EI}}. \tag{16}$$

The computation of the integrals associated with this formulation is carried out using the Gauss–Legendre quadrature with the `gauleg` algorithm,[40] with a minimum of 15 integration points per wavelength. Note that in contrast with the plane wave approximation equation (10) which can comprise an arbitrary number of terms, the number of the enrichment functions in Eq, (13) is constant. As a result, the so-called p-refinement strategy, i.e. by increasing the number of approximating functions, is not feasible and convergence analysis can only be performed using h-refinement, i.e. by decreasing the element size. The specific choice in relation to Eq. (15) is based on recent results in Ref. 28, which demonstrate that it should provide best convergence rates for *in vacuo* problems when the coupling with a fluid is ignored.

2.4. *Guidelines for the computation of PUFEM matrix coefficients, mesh size and vibro-acoustic coupling*

As discussed earlier in previous papers from the authors,[23] PUFEM elements in the acoustic domain are designed to span over many wavelengths. In some cases, small geometric features might limit the element size but PUFEM elements can still provide accurate solutions, although the performance, in terms of data reduction, may not be optimal.[26] On the contrary, beam elements with PUFEM approximation (Eq. (13)) remain very accurate as long as the element size h_s does not exceed a typical wavelength of the vibrating structure, defined as $\lambda_s = 2\pi/k_s$. This is illustrated in Fig. 2, which shows the convergence rate of an *in vacuo* beam subject to a uniform loading. Here, the error is computed using the $\mathcal{L}_2$-norm and the reference solution is calculated using classical modal expansion method. It appears indeed that as long as $h_s \approx \lambda_s$, errors are below $10^{-2}\%$ and they decrease for higher frequencies. These observations motivate us to consider two coupling strategies using either a compatible mesh or an incompatible mesh. Coupling integrals in Eqs. (8) and (9) are of the

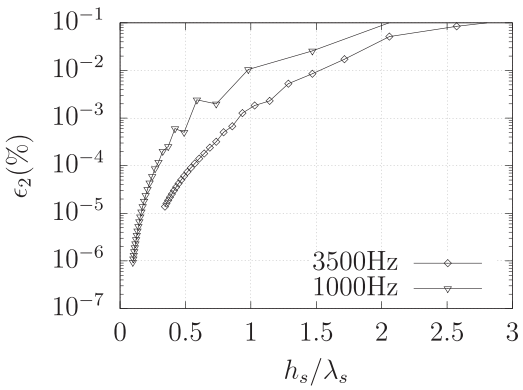

Fig. 2. Convergence of the *in vacuo* beam.

general form

$$I = \int_{\Gamma_s} X_w X_p \mathrm{d}\Gamma, \tag{17}$$

where function X_w denotes either the real w and virtual displacement δw and similarly with the acoustic load $X_p = p$ or $X_p = \delta p$. Given that $\Gamma_s = \bigcup_{m=1}^{M} \Gamma_s^m$, this integral is mapped onto the reference element of the beam giving

$$I = \sum_{m=1}^{M} \int_{-1}^{1} X_w(\mu) X_p(\xi(\mu)) J \mathrm{d}\mu, \tag{18}$$

where J is the Jacobian of the geometric transformation and the function $\xi(\mu)$ expresses the connection between the two coordinate systems associated with the beam element Γ_s^m and the edge of an acoustic PUFEM element Γ_f^i which share a common boundary as illustrated in Fig. 3. When elements are compatible then we have simply $\xi(\mu) = \mu$. The integral in Eq. (18) is computed using the Gauss–Legendre quadrature with 15 points of integration per $\min(\lambda_s, \lambda_f)$, where λ_s, λ_f are the wavelengths of the structure and of the fluid, respectively.

3. Convergence Analysis

The method is tested for a test case, described in Fig. 4, which consists of 1 m sided square-shaped cavity enclosed with three rigid walls and backed by a simply supported beam.

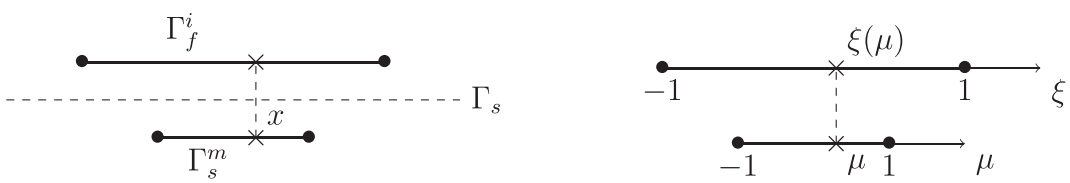

Fig. 3. Example of elements of an incompatible mesh. On the left elements in the global coordinate system; on the right elements in their respective local coordinate system.

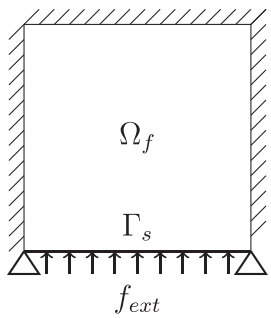

Fig. 4. Test case which consist of a 1 m sided square-shaped cavity backed by a simply supported beam.

Table 1. Physical properties.

(a) Structure		(b) Fluids		
	Structure		Air	Water
E	70 GPa	ρ_f	$1.23\,\mathrm{kg\cdot m^{-3}}$	$1000\,\mathrm{kg\cdot m^{-3}}$
ρ	$2780\,\mathrm{kg\cdot m^{-3}}$	c_f	$340\,\mathrm{m\cdot s^{-1}}$	$1480\,\mathrm{m\cdot s^{-1}}$
d	1 cm			
b	1 cm			
Q	$1 \sim 10^{-5}\,\mathrm{N/m}$			

Physical properties of the beam are defined in Table 1(a). Two types of fluids, air and water, are considered with their properties tabulated in Table 1(b).

As stated previously, the tuning parameter C in Eq. (12) is usually chosen in the interval $[2, 20]$. The following convergence analysis has been performed for different C and $C = \{6, 8, 10\}$ provided best results. The results presented in this section are those corresponding to $C = 8$.

The convergence analysis is performed for different mesh refinement strategies and performances are measured with the $\mathcal{L}_2$-norm errors in terms of both the acoustic pressure and the displacement as

$$\epsilon_{2,p} = \frac{\|p - \hat{p}\|_{\mathcal{L}_2(\Omega_f)}}{\|\hat{p}\|_{\mathcal{L}_2(\Omega_f)}} \quad \text{and} \quad \epsilon_{2,w} = \frac{\|w - \hat{w}\|_{\mathcal{L}_2(\Gamma_s)}}{\|\hat{w}\|_{\mathcal{L}_2(\Gamma_s)}}, \tag{19}$$

where the reference solutions $\hat{p}$ and $\hat{w}$ are computed using a modal expansion method based on the notion of coupled modes as explained in Ref. 41 and, for completeness, all necessary details are given in Appendix A.

Refinement strategies differ depending on the vibro-acoustic coupling strategy. With compatible meshes, two refinement strategies are used. The first one, which is also the simplest, uses structured meshes, whereby the size of the elements in the acoustic domain are constrained by the size of the beam elements so that the mesh refinement is entirely controlled by the discretization of the beam (see Fig. 5(a)). The second strategy uses compatible unstructured meshes whereby the mesh in the acoustic domain gradually become

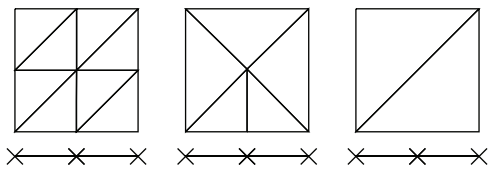

Fig. 5. Second to coarser meshes of the refinement process. (a) Structured compatible meshes, (b) unstructured compatible meshes and (c) incompatible meshes.

coarser when getting away from the fluid–structure interface. Here, the refinement of the mesh is mainly active in the vicinity of the interface. With incompatible meshes the refinement strategy can be carried out independently which means that PUFEM elements in the acoustic domain are built so that they can span over many wavelengths whereas the beam is discretized with the rule that the size of the beam element should not exceed 1 or 2 wavelengths as discussed earlier in Sec. 2.4. It is relevant to note that during the refinement process with incompatible meshes, only the number of elements of the vibrating structure increases while the acoustic mesh remains unchanged (see Fig. 5(c)).

First, the convergence analysis is carried out at $f = 3500\,\text{Hz}$ with air as fluid. At this frequency, the length of the beam verifies $L/\lambda_s = 6.25$ and $L/\lambda_f = 10.3$ which signifies that the wave field exhibits many oscillations in the computational domain and the PUFEM is expected to perform well in this context. Figures 6(a) and 6(b) show the convergence for both the acoustic pressure and the displacement of the beam. The first three curves correspond to the computed results with compatible structured meshes, compatible unstructured meshes and incompatible meshes, respectively, while the last curve with classical FEM with cubic Hermite elements for the beam and quadratic elements in the acoustic domain. Clearly, the PUFEM with different meshing strategies all outperforms the classical FEM irrespective of the type of mesh refinement used. Indeed, in some cases, the use of FEM necessitates up to 10^3 times more DoF in order to reach the same level of accuracy as PUFEM. It can also be observed that compatible unstructured meshes permit faster convergence than compatible structured meshes. This observation is not surprising since the application of PUFEM in the acoustic domain is best suited for larger elements which occur far from the coupling interface with unstructured meshes contrary to structured ones. The same arguments can be used to explain why incompatible meshes give the best results: here an error in the order of magnitude of $10^{-4}\%$ with 500 DoF can be reached, while more than twice as many DoF are required with other techniques. From these observations, some conclusions can be drawn about the validity of the guidelines stated earlier. Indeed, the frequency (here 3500 Hz) is sufficiently high, so the criteria that the mesh size in the acoustic domain should be chosen to be larger than a typical wavelength, i.e. $h_f \geq \lambda_f$, is satisfied in all cases. However, the other condition that h_s should not exceed the size of wavelength λ_s is not necessarily met. To demonstrate this, the computational scenarios which correspond to the condition that $h_s = \lambda_s$ is highlighted with a red bullet in Figs. 6(a) and 6(b). This shows that once this condition is satisfied the level of error becomes highly satisfactory regardless of the coupling strategy.

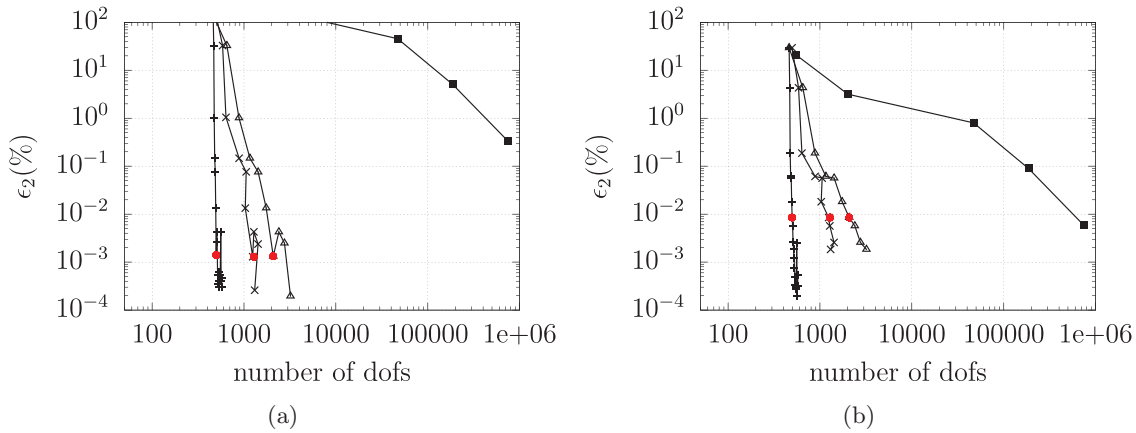

Fig. 6. Convergence of the methods at $f = 3500\,\text{Hz}$. *Notes*: —△— compatible structured; —×— compatible unstructured; —+— incompatible; —■— quadratical FEM. (a) Acoustic domain and (b) structure domain.

In order to illustrate the different meshing strategies, the acoustic pressure fields in the cavity (calculated with the meshes corresponding to the red bullet) are shown in Fig. 7. The displacement field w of the beam is also plotted. In the case of the compatible structured mesh (cf. Fig. 7(a)), the size of the elements in the acoustic domain are roughly equal to the acoustic wavelength and the PUFEM is not optimal in terms of data reduction. Better performances are observed with compatible unstructured meshes (cf. Fig. 7(b)), as expected, due to the presence of larger elements away from the interface. Finally, the use of incompatible meshes (cf. Fig. 7(c)) allows elements in the acoustic domain to be free from size constraints and this permits to take full advantage of the method.

The case of heavy fluid (water) at high frequency, $f = 35\,\text{kHz}$, is now examined.[a] The presence of the water, as a dense fluid, exerts increasing fluid loading on the beam, and in the meantime, increases the coupling strength with the plate through its sound radiation. In this scenario, wavelengths are $\lambda_s = 0.05\,\text{m}$ and $\lambda_f = 0.04\,\text{m}$. Convergence curves are shown in Fig. 8. The same behavior as in Figs. 6(a) and 6(b) is observed though what distinguishes the three meshing strategies is amplified by the fact that the number of oscillations in the beam is three times higher than in the previous study, see Fig. 9. Once again, the use of incompatible meshes provides the best computational efficiency. It appears that in this configuration the overall accuracy is lower than in Fig. 6. Since all methods floor at the same level error (between $10^{-3}\%$ and $10^{-2}\%$) authors suspect that at such a high frequency the reference solution does not converge as well as at lower frequencies.

[a]At such a high frequency, the elastodynamic behavior of the beam would be better captured using the Timoshenko beam theory. Yet, no reference solution exists for the problem at stake using Timoshenko formulation. To study the convergence of the present method the Euler–Bernoulli theory is kept for the numerical model and for the reference solution. Adapting the present numerical method to a Timoshenko beam is straightforward using[27] since the coupling method remains unchanged.

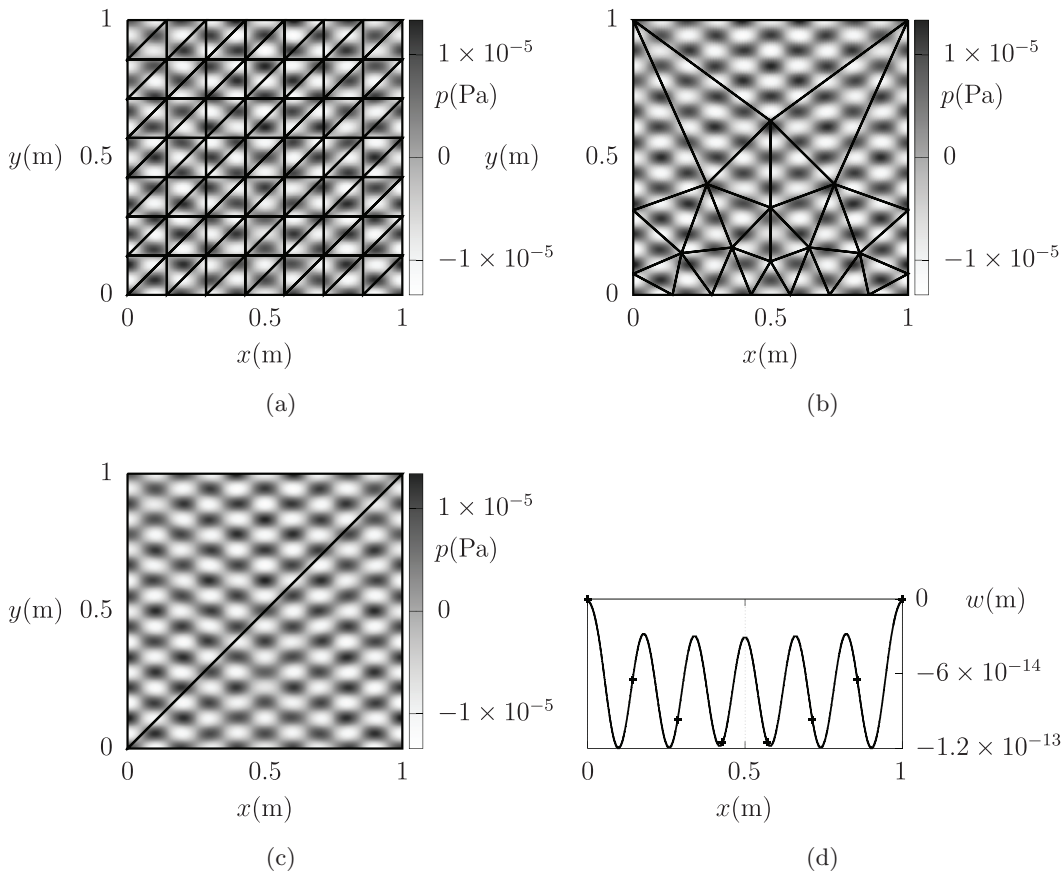

Fig. 7. Fields at $f = 3500\,\text{Hz}$ with the different methods. Fluid: air. In the acoustic domain, meshes appear in black lines. (a) Pressure; compatible structured, (b) pressure; compatible unstructured, (c) pressure; incompatible and (d) displacement field. Nodes of the mesh are marked with black plus signs.

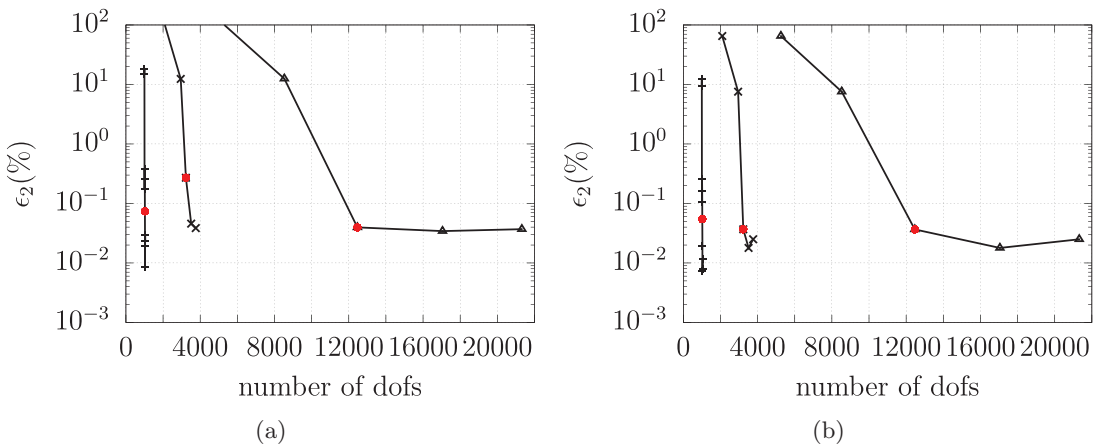

Fig. 8. Convergence at $f = 35\,\text{kHz}$. *Notes*: —▲— compatible structured; —×— compatible unstructured; —+— incompatible. (a) Acoustic and (b) structure.

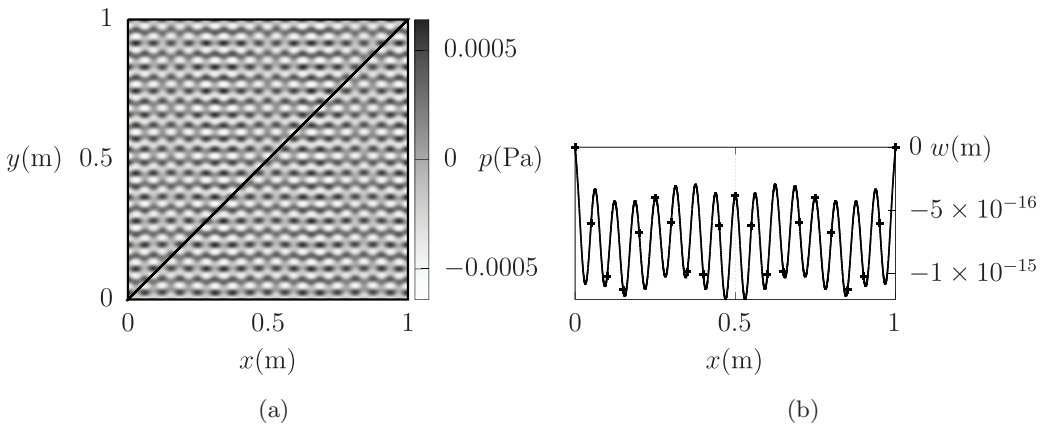

Fig. 9. Fields at $f = 35\,\text{kHz}$, coupled with water, 20 elements along the beam. (a) Pressure field and (b) displacement field.

Previous calculations were carried out in rather high-frequency ranges, where the PUFEM is well suited. These frequency ranges lie above the critical frequency of the beam (24 109 Hz in water in the present case), meaning that the wavelength is smaller in the fluid domain than in the structure domain. A brief study is now carried out below the critical frequency, at 5 kHz with water as fluid. Convergence curves for both domains are given in Fig. 10. Unlike previous results, the incompatible method does not stand out as the best overall. Indeed, with this method, the error quickly drops to $10^{-1}\%$ to $10^{-2}\%$. Then, as the number of DOF increases, the error becomes slightly unstable (oscillating between $10^{-2}\%$ and 1%). This comes from the fact that in such a situation, acoustic elements must capture the evanescent character of the wave field in the vicinity of the beam. Although the plane wave basis with propagating plane waves can theoretically simulate evanescent waves, numerical limitations due to the finite machine precision can sometimes occur[42] and this is

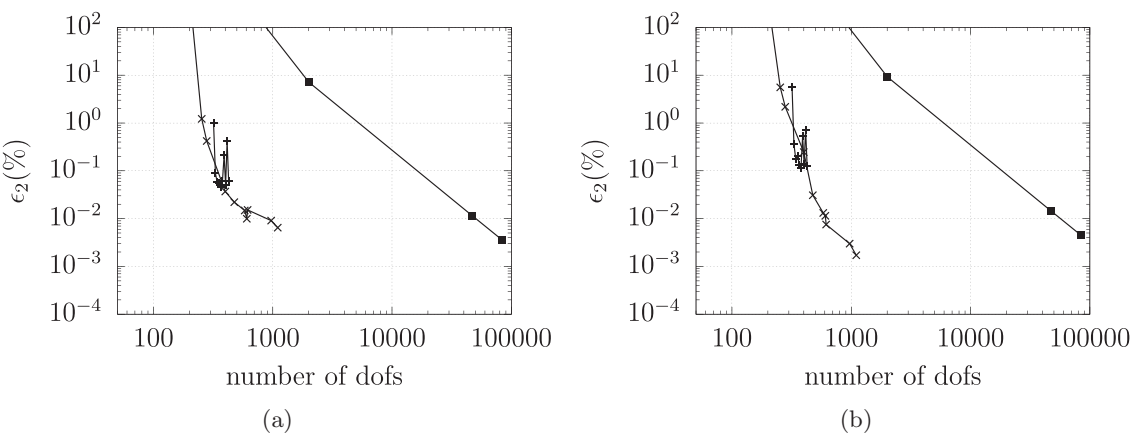

Fig. 10. Convergence at $f = 5000\,\text{Hz}$. *Notes*: compatible unstructured; incompatible; FEM. (a) Acoustic and (b) structure.

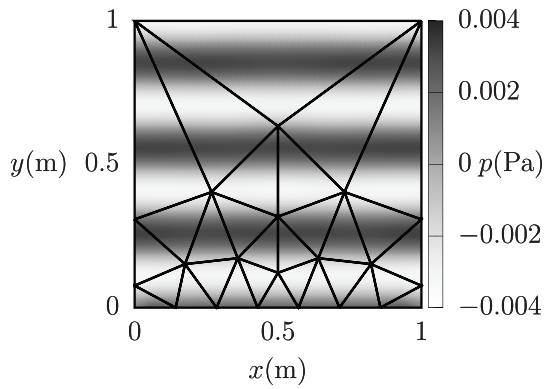

Fig. 11. Pressure field at 5000 Hz. Fluid: water. Compatible unstructured mesh appears in black lines.

reflected here by a slight loss of accuracy. In the context of the PUFEM for modeling flexural waves, improvements can be made by using hybrid enrichments with both propagating plane waves and high-order polynomials.[28] Another strategy consists in refining the acoustic mesh near the vibrating structure. This is the case with the compatible unstructured mesh, for which the element size is smaller in the vicinity of the coupling interface, as illustrated in Fig. 11, where evanescent waves are located. This explains why the compatible unstructured mesh method performs better. Note that in general the PUFEM is not dedicated to such relatively low-frequency ranges. Nevertheless, it still performs very well in terms of accuracy with the unstructured compatible mesh, as illustrated in Fig. 10.

Before we leave this section we may note that, from a practical point view, the use of structured and compatible meshes is the most straightforward way whereas mesh tweaking is needed with the unstructured mesh. Indeed, unstructured meshes are generated using `gmsh`[43] by setting an average element size in the structure domain and declaring both vertical walls of the acoustic domain as *Transfinite Lines*. At each step of the refinement process, the average element size in the structure domain is reduced and the element progression along the *Transfinite Lines* is manually set. This is a tedious work which requires a sense of PUFEM behavior to avoid excessive size difference between adjacent acoustic elements. Finally, the method using incompatible meshes, which requires more attention at the implementation stage, facilitates the mesh preparation and yields best performances.

4. Application

The aim of this section is to show that the method presented in this work is suited to model real-life 2D problems with increasing complexity. The configuration under investigation is described in Fig. 12 and Table 2. It consists of a hollow vessel (air inside) submerged in water. The vessel consists of two horizontal straight portions (modeled as beams simply supported at both ends), closed by two rigid circular end caps. For a brief nomenclature, subscript w (respectively, a) refers to the water (respectively, air) domain whereas subscript s refers to the vibrating structure. The latter is excited by a point force acting on point

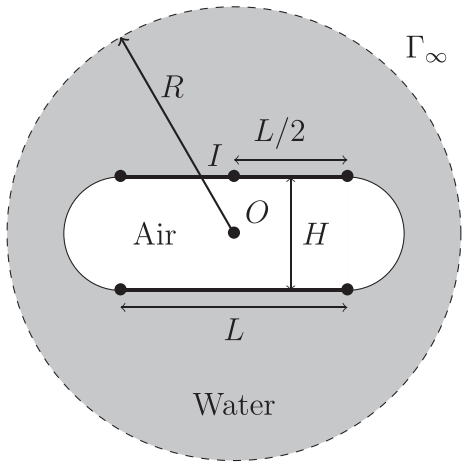

Fig. 12. Vessel configuration.

Table 2. Dimensions.

	Dimension (m)
R	1
L	1
H	0.5

I as shown in Fig. 12. The water domain is considered as infinite with an NRBC on the external Γ_∞. The latter has been chosen to have a circular shape centered on point O with a radius R so the outgoing acoustic pressure can be expressed as a series of harmonics which yields the following Dirichlet-to-Neumann (DtN) operator[44]:

$$Bp = \frac{k_w}{2\pi}\sum_{n=0}^{\infty}(2-\delta_{n0})\frac{H_n'(k_wR)}{H_n(k_wR)}\int_0^{2\pi} p(R,\theta')\cos n(\theta-\theta')\mathrm{d}\theta' \quad \text{on } \Gamma_\infty. \tag{20}$$

Here, B is the boundary operator as defined in the Robin general condition Eq. (2), δ_{n0} is the Kronecker delta function and H_n is the Hankel function of the first kind. Equation (20) contains an infinite sum which has to be truncated. To do so, the criterion $N = k_wR$ given in Ref. 45 is used, which was shown to provide sufficiently accurate results. Note that this type of NRBC has already been studied in the framework of the PUFEM in Ref. 25.

PUFEM simulations are carried out at $f = 7000\,\mathrm{Hz}$ with $\lambda_s = 0.11\,\mathrm{m}$. The element length is set to 0.1 m, yielding 10 beam elements in the discretization. In the water domain and the air domain, wavelengths are $\lambda_w = 0.21\,\mathrm{m}$ and $\lambda_a = 0.049\,\mathrm{m}$, respectively. The coupling method with incompatible mesh is used and acoustic elements are chosen to be as large as possible whenever feasible to preserve the computational performances of the PUFEM. In fact, the limitation mainly stems from the need to minimize geometrical error near the curved boundaries (recall that the geometry of elements is mapped with quadratic shape functions) and this can have a detrimental effect on the overall accuracy especially

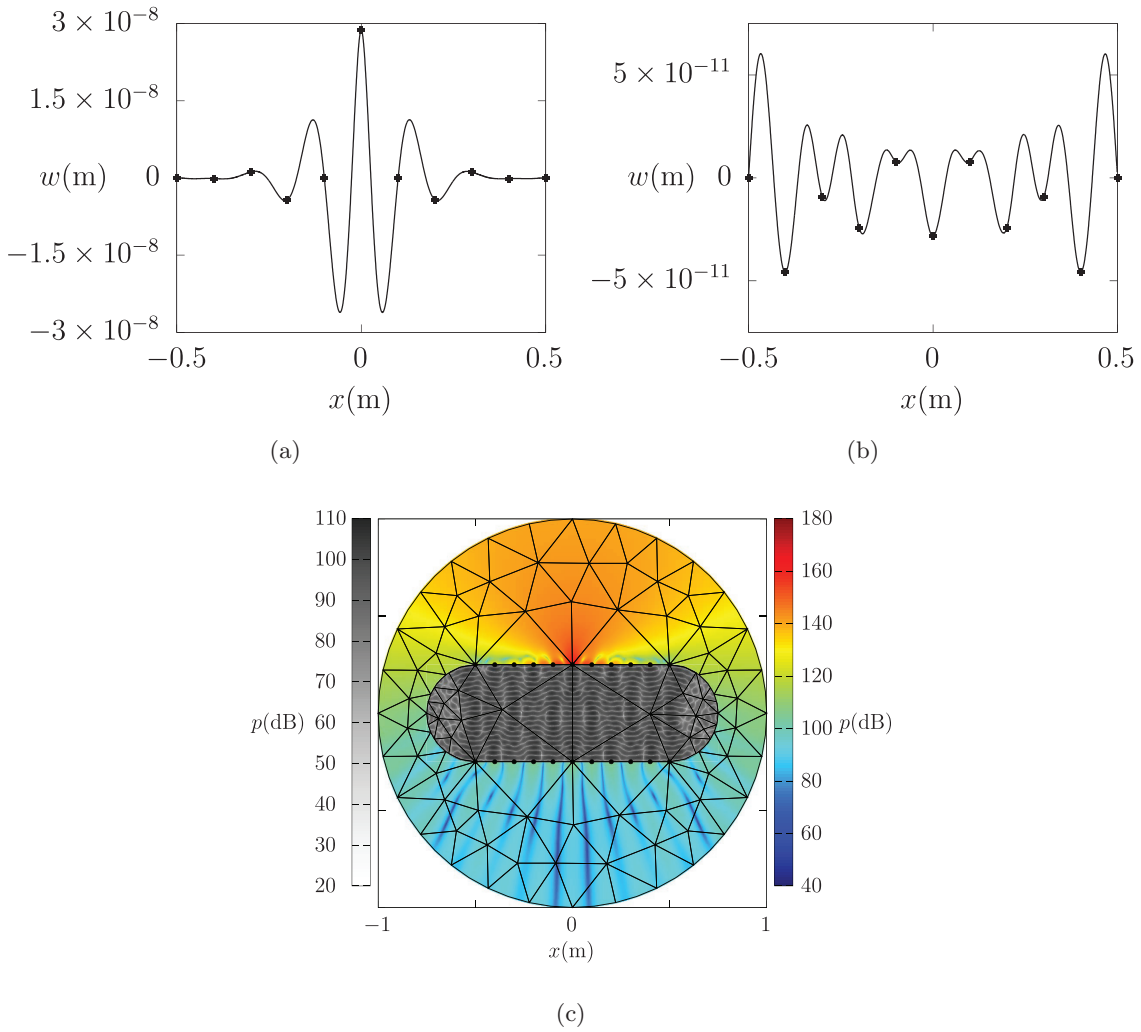

Fig. 13. Fields at $f = 7\,\text{kHz}$. (a) Displacement of the top beam — excited with a point force, (b) displacement of the bottom beam and (c) pressure fields in dB. Left color bar corresponds to the pressure in the vessel; right color bar corresponds to the pressure outside of the vessel.

as the wavelength shortens. Figure 13(c) shows the acoustic pressure inside and outside the vessel. Since the vessel is filled with air, wavelengths are substantially smaller than in the external fluid. The highly oscillatory wave field in the vessel is well captured by the PUFEM elements which can span over several wavelengths (up to 10), which signifies that the method is well suited for the present test case. In the surrounding water, the geometrical constraints due the curved shape of the inner and outer boundaries and the fact that the sound speed is nearly five times larger restrict the size of the elements compared to the wavelength. Thanks to the incompatible mesh, elements near the coupling interface are substantially larger and are able to simulate the standing waves which are present in the vicinity of the vibrating structure. In Fig. 13(a) is plotted the displacement field of the top portion of the vessel

Table 3. Convergence of the vessel model in fluid domains ($C_a = 4$).

C_w	Number of DOF	$\tilde{\epsilon}_{2,p}$ water (%)	$\tilde{\epsilon}_{2,p}$ air (%)
4	2746	91.923	87.377
6	3072	16.275	6.826
8	3402	3.517	1.816
10	3712	0.0692	0.848
12	4038	0.0567	0.858

showing a maximum at point I ($x = 0$) where the excitation point force is applied. The displacement field of the bottom portion is also shown in Fig. 13(b), where each element can capture approximately a full wavelength. The vibrational level of the bottom portion vessel which results from the inner and outer acoustic loading is significantly smaller than the top one.

Assessing the quality of the model in such a configuration is difficult since, to authors knowledge, no analytical solution exists. To quantify it at a low computational cost in fluid domains, the error estimator (Eq. (37) from Ref. 22) is used. This estimator states that if no energy is lost (no damping and no NRBC) the imaginary part of the pressure should be zero so the quality of the PUFEM model can be assessed using the following equation:

$$\tilde{\epsilon}_{2,p} = \frac{\|\mathrm{Im}(p)\|_{\mathcal{L}_2(\Omega_f)}}{\|\mathrm{Re}(p)\|_{\mathcal{L}_2(\Omega_f)}}. \tag{21}$$

Using the above, the DtN has to be replaced by a rigid boundary condition. Trying several C_w, which controls the level of the discretization in Eq. (12), in the water domain, allows to find the value of C_w at which the model has converged. This analysis is presented in Table 3. Here, one can observe that with $C_w = 10$, the model produces a very low error in the water domain and the air domain, 0.069% and 0.85%, respectively. In addition, the gain in accuracy from $C_w = 10$ to $C_w = 12$ is small, which indicates that the acoustic model has converged and further discretizing would not improve the quality significantly. To ensure that the model has converged on the structure side, similar techniques as those deployed in FEM can be used. For instance, h-refinement can be performed. As mentioned before, in this configuration, each beam has been partitioned into 10 elements. A second calculation is carried out with 20 elements in each beam. The $\mathcal{L}_2$-norm difference between the two calculations is 0.006% and 0.025% for the top and the bottom beam, respectively. Such a small difference indicates that the model with 10 elements in each beam has indeed converged, further refining of the structure domain is unnecessary.

5. Conclusion

This paper contributes to the numerical modeling of 2D fluid–structure coupling problems in the mid-to-high frequency range. Using PUFEM in both fluid and structure domains, we show that the method outperforms conventional FEM in terms of number of DoF required to achieve a prescribed computational accuracy. We also show that the method produces

accurate results no matter whether the fluid is light or heavy, thus reflecting different coupling strength with a vibrating structure. Knowing that the PUFEM is less efficient in the structure domain than in the acoustic domain in terms of number of wavelength captured by a single element, several coupling strategies have been proposed and investigated. The one involving incompatible meshes singles out as the most efficient one above the critical frequency of the structure, and the easiest one to use. Below the critical frequency, incompatible meshes are still accurate with typically 0.1% of error, but compatible meshes with a refined mesh at the coupling interface are slightly better in this case in order to accurately capture both propagating and evanescent waves.

In addition, meshing guidelines have been provided and validated through convergence analyses. These guidelines stipulate that to reach accurate results while maintaining a low number of DoF: (i) the element length in the structure domain should be inferior or equal to the *in vacuo* wavelength of the structure; (ii) the average element length in the acoustic domain should be larger than one wavelength. Finally, through an application to a 2D vessel problem, we demonstrated the applicability of the method to more elaborate problems. Results show the efficacy of the proposed method, as well as the wealth of information and physical details that it can offer.

This paper being the first to tackle vibro-acoustic problems using PUFEM for both the acoustics and the elastodynamics, perspectives can be drawn from it. It appears that investigations could be carried out to enhance the performance of the method below the critical frequency where the vibration of the beam creates evanescent acoustic waves. Including evanescent waves in the approximation basis has been done in acoustics[46] and in elastodynamics[28] to better capture evanescent waves. This remains to be done in the coupled case. Then the natural evolution of this work would be to extend it to the 3D case. In that case, the plate model developed in Ref. 28 allows to perform p-refinement so different conclusions are to be expected.

Acknowledgments

Authors thank the French ministry "*Ministère de l'Enseignement Supérieur, de la Recherche et de l'Innovation*" along with the "*Région des Hauts de France*" for financing this research. The third author also thank the support from the Research Grant Council of the Hong Kong SAR (PolyU 152017/17E).

References

1. M. Petyt, *Introduction to Finite Element Vibration Analysis*, 2nd edn. (Cambridge University Press, 2010).
2. P. K. Banerjee and R. Butterfield, *Boundary Element Methods in Engineering Science*, Vol. 17 (McGraw-Hill, London, 1981).
3. F. Ihlenburg and I. Babuska, Finite element solution to the Helmholtz equation with high wave number. Part 1: The h-version of the FEM, Technical report (1993).

4. P. Bouillard and F. Ihlenburg, Error estimation and adaptivity for the finite element method in acoustics, in *Advances in Adaptive Computational Methods in Mechanics* (Elsevier, 1998), pp. 477–492.
5. A. Deraemaeker, I. Babuška and P. Bouillard, Dispersion and pollution of the fem solution for the Helmholtz equation in one, two and three dimensions, *Int. J. Numer. Methods Eng.* **46**(4) (1999) 471–499.
6. C. Soize, A model and numerical method in the medium frequency range for vibroacoustic predictions using the theory of structural fuzzy, *J. Acoust. Soc. Am.* **94**(2) (1993) 849–865.
7. R. S. Langley and P. Bremner, A hybrid method for the vibration analysis of complex structural–acoustic systems, *J. Acoust. Soc. Am.* **105**(3) (1999) 1657–1671.
8. K. Vergote, B. Van Genechten, D. Vandepitte and W. Desmet, On the analysis of vibro-acoustic systems in the mid-frequency range using a hybrid deterministic-statistical approach, *Comput. Struct.* **89**(11) (2011) 868–877; Computational Fluid and Solid Mechanics.
9. B. F. Shorr, *The Wave Finite Element Method* (Springer, Berlin, Heidelberg, 2004).
10. E. Chadwick and P. Bettess, Modelling of progressive short waves using wave envelopes, *Int. J. Numer. Methods Eng.* **40**(17) (1997) 3229–3245.
11. C. Farhat, I. Harari and L. P. Franca, The discontinuous enrichment method, *Comput. Methods Appl. Mech. Eng.* **190**(48) (2001) 6455–6479.
12. C. Farhat, I. Harari and U. Hetmaniuk, A discontinuous Galerkin method with Lagrange multipliers for the solution of Helmholtz problems in the mid-frequency regime, *Comput. Methods Appl. Mech. Eng.* **192**(11) (2003) 1389–1419.
13. G. Gabard and O. Dazel, A discontinuous Galerkin method with plane waves for sound-absorbing materials, *Int. J. Numer. Methods Eng.* **104**(12) (2015) 1115–1138.
14. W. Desmet, B. van Hal, P. Sas and D. Vandepitte, A computationally efficient prediction technique for the steady-state dynamic analysis of coupled vibro-acoustic systems, *Adv. Eng. Softw.* **33**(7) (2002) 527–540; Engineering Computational Technology & Computational Structures Technology.
15. E. Deckers, O. Atak, L. Coox, R. D'Amico, H. Devriendt, S. Jonckheere, K. Koo, B. Pluymers, D. Vandepitte and W. Desmet, The wave based method: An overview of 15 years of research, *Wave Motion* **51**(4) (2014) 550–565.
16. P. Rouch and P. Ladevèze, The variational theory of complex rays: A predictive tool for medium-frequency vibrations, *Comput. Methods Appl. Mech. Eng.* **192**(28) (2003) 3301–3315; Multiscale Computational Mechanics for Materials and Structures.
17. Katholieke Universiteit te Leuven (O. Atak, B. Pluymers and W. Desmet), *MID-FREQUENCY — CAE Methodologies for Mid-Frequency Analysis in Vibration and Acoustics* (Katholieke Universiteit Leuven, Faculty of Engineering, 2012).
18. I. Babuska and J. M. Melenk, The partition of unity finite element method, Technical report (1995).
19. J. M. Melenk and I. Babuška, The partition of unity finite element method: Basic theory and applications, *Comput. Methods Appl. Mech. Eng.* **139**(1–4) (1996) 289–314.
20. O. Laghrouche, P. Bettess, E. Perrey-Debain and J. Trevelyan, Plane wave basis finite-elements for wave scattering in three dimensions, *Commun. Numer. Methods Eng.* **19**(9) (2003) 715–723.
21. P. Bettess, J. Shirron, O. Laghrouche, B. Peseux, R. Sugimoto and J. Trevelyan, A numerical integration scheme for special finite elements for the Helmholtz equation, *Int. J. Numer. Methods Eng.* **56**(4) (2002) 531–552.
22. M. Yang, E. Perrey-Debain, B. Nennig and J.-D. Chazot, Development of 3D PUFEM with linear tetrahedral elements for the simulation of acoustic waves in enclosed cavities, *Comput. Methods Appl. Mech. Eng.* **335** (2018) 403–418.

23. J.-D. Chazot, B. Nennig and E. Perrey-Debain, Performances of the partition of unity finite element method for the analysis of two-dimensional interior sound fields with absorbing materials, *J. Sound Vib.* **332**(8) (2013) 1918–1929.
24. J.-D. Chazot, E. Perrey-Debain and B. Nennig, The partition of unity finite element method for the simulation of waves in air and poroelastic media, *J. Acoust. Soc. Am.* **135**(2) (2014) 724–733.
25. O. Laghrouche, A. El-Kacimi and J. Trevelyan, A comparison of NRBCs for PUFEM in 2D Helmholtz problems at high wave numbers, *J. Comput. Appl. Math.* **234**(6) (2010) 1670–1677.
26. C. Langlois, J.-D. Chazot, E. Perrey-Debain and B. Nennig, Partition of unity finite element method applied to exterior problems with perfectly matched layers, *Acta Acust.* **4**(4) (2020) 16.
27. T. Zhou, J.-D. Chazot, E. Perrey-Debain and L. Cheng, Performance of the partition of unity finite element method for the modeling of Timoshenko beams, *Comput. Struct.* **222** (2019) 148–154.
28. T. Zhou, J.-D. Chazot, E. Perrey-Debain and L. Cheng, Modeling of thin plate flexural vibrations by partition of unity finite element method, *Int. J. Appl. Mech.* **13** (2021) 2150030.
29. A. El Kacimi and O. Laghrouche, Numerical modelling of elastic wave scattering in frequency domain by the partition of unity finite element method, *Int. J. Numer. Methods Eng.* **77**(12) (2009) 1646–1669.
30. E. De Bel, P. Villon and P. Bouillard, Forced vibrations in the medium frequency range solved by a partition of unity method with local information, *Int. J. Numer. Methods Eng.* **62**(9) (2005) 1105–1126.
31. A. El Kacimi and O. Laghrouche, Improvement of PUFEM for the numerical solution of high-frequency elastic wave scattering on unstructured triangular mesh grids, *Int. J. Numer. Methods Eng.* **84** (2010) 330–350.
32. T. Zhou, J.-D. Chazot, E. Perrey-Debain and L. Cheng, Partition of unity finite element method for the modelling of acoustic black hole wedges, *J. Sound Vib.* **475** (2020) 115266.
33. M. Dinachandra and S. Raju, Plane wave enriched partition of unity isogeometric analysis (PUIGA) for 2D-Helmholtz problems, *Comput. Methods Appl. Mech. Eng.* **335** (2018) 380–402.
34. G. C. Diwan and M. Shadi Mohamed, Pollution studies for high order isogeometric analysis and finite element for acoustic problems, *Comput. Methods Appl. Mech. Eng.* **350** (2019) 701–718.
35. M. Drolia, M. S. Mohamed, O. Laghrouche, M. Seaid and A. El Kacimi, Explicit time integration with lumped mass matrix for enriched finite elements solution of time domain wave problems, *Appl. Math. Model.* **77** (2020) 1273–1293.
36. P. Bouillard, V. Lacroix and E. De Bel, A wave-oriented meshless formulation for acoustical and vibro-acoustical applications, *Wave Motion* **39**(4) (2004) 295–305.
37. Z. Li, P. Li, Z. He and G. Liu, Coupled partition of unity method and improved meshless weighted least-square method for two-dimensional interior structure–acoustic problem, *Eng. Anal. Bound. Elem.* **36**(2) (2012) 154–160.
38. T. Huttunen, P. Gamallo and R. J. Astley, Comparison of two wave element methods for the Helmholtz problem, *Commun. Numer. Methods Eng.* **25**(1) (2009) 35–52.
39. E. Perrey-Debain, O. Laghrouche, P. Bettess and J. Trevelyan, Plane-wave basis finite elements and boundary elements for three-dimensional wave scattering, *Philos. Trans. R. Soc. Lond. A, Math. Phys. Eng. Sci.* **362**(1816) (2004) 561–577.
40. W. Press, S. Teukolsky, W. Vetterling and B. Flannery, *Numerical Recipes in Fortran 90*: *The Art of Parallel Scientific Computing*, Vol. 2 (Press Syndicate of the University of Cambridge, 1997).
41. R. W. Guy and M. C. Bhattacharya, The transmission of sound through a cavity-backed finite plate, *J. Sound Vib.* **27**(2) (1973) 207–223.

42. E. Perrey-Debain, Plane wave decomposition in the unit disc: Convergence estimates and computational aspects. *J. Comput. Appl. Math.* **193**(1) (2006) 140–156.
43. C. Geuzaine and J.-F. Remacle, Gmsh: A 3-D finite element mesh generator with built-in pre- and post-processing facilities, *Int. J. Numer. Methods Eng.* **79**(11) (2009) 1309–1331.
44. D. Givoli and S. Vigdergauz, Artificial boundary conditions for 2D problems in geophysics, *Comput. Methods Appl. Mech. Eng.* **110**(1) (1993) 87–101.
45. I. Harari and T. J. R. Hughes, Analysis of continuous formulations underlying the computation of time-harmonic acoustics in exterior domains, *Comput. Methods Appl. Mech. Eng.* **97**(1) (1992) 103–124.
46. K. Christodoulou, O. Laghrouche, M. S. Mohamed and J. Trevelyan, High-order finite elements for the solution of Helmholtz problems, *Comput. Struct.* **191**(1) (2017) 129–139.

Appendix A. Analytical Solution

To solve analytically the problem described in Fig. 4, the method described in Ref. 41 is used. Boundary conditions for this problem are

$$\begin{cases} \left.\dfrac{\partial p}{\partial n}\right|_{x=0} = \left.\dfrac{\partial p}{\partial n}\right|_{x=L} = \left.\dfrac{\partial p}{\partial n}\right|_{y=L} = 0, & \text{(A.1)} \\ w(0) = w(L) = 0, & \text{(A.2)} \\ \left.\dfrac{\partial p}{\partial n}\right|_{\Gamma_s} = -\omega^2 \rho_f w. & \text{(A.3)} \end{cases}$$

Equation (A.1) imposes a rigid boundary condition, Eq. (A.2) imposes that both ends of the beam are pinned and Eq. (A.3) imposes the speed continuity between both domains at the interface. The aim is to solve this coupled problem by determining w and p. To do so, the transverse displacement is expressed as an infinite sum of *in vacuo* modes with an unknown amplitude:

$$w = \sum_{r=1}^{\infty} \sin k_r x W_r, \tag{A.4}$$

where $k_r = r\pi/L$ and W_r is the amplitude of mode r. Then the pressure is expressed as a sum of function which all verify Eq. (A.1) and $\left.\frac{\partial p}{\partial n}\right|_{y=0} \neq 0$:

$$p = \sum_{m=0}^{\infty} \Phi_m P_m \quad \text{where } \Phi_m = \cos k_m x \, \frac{\cosh \mu_m (L-y)}{\mu_m \sinh \mu_m L} \quad \text{and} \quad \mu_m = \sqrt{k_m^2 - k_f^2}, \tag{A.5}$$

where P_m is the amplitude of Φ_m. The pressure p has to verify the coupling boundary condition equation (A.3). To enforce this, the coupling equation (A.3) is written using

Eqs. (A.4) and (A.5) which leads to

$$\sum_{m=0}^{\infty} \cos k_m x P_m = -\omega^2 \rho_f \sum_{r=0}^{\infty} \sin k_r x W_r, \tag{A.6}$$

weighting Eq. (A.6) with $\cos k_n x$ and integrating over $x \in [0, L]$ leads to

$$P_n \frac{L}{2}(1 + \delta_n) = -\rho_f \omega^2 \sum_{r=0}^{\infty} \Delta_{nr} W_r, \tag{A.7}$$

where

$$\Delta_{nr} = \begin{cases} 0 & \text{if } n = r, \\ \dfrac{1 - (-1)^{n+r}}{2(k_n + k_r)} - \dfrac{1 - (-1)^{|n-r|}}{2(k_n - k_r)} & \text{otherwise.} \end{cases} \tag{A.8}$$

This equations provides a relationship between P_n and W_r, a second is needed to be able to solve the problem. The second relationship is obtained by taking into account the participation of the acoustic pressure in the governing equation of the beam's transverse displacement:

$$EI \frac{\partial^4 w}{\partial x^4} - \omega^2 \rho_s S w = f_{\text{ext}} - pb. \tag{A.9}$$

Then Eq. (A.9) is weighed with a mode Φ_q and is integrated for $x \in [0, L]$ which leads to

$$(EI k_q^4 - \rho_s S \omega^2) \frac{L}{2} W_q = f_{\text{ext}} \frac{1 - (-1)^q}{k_q} - b \sum_{n=0}^{\infty} \frac{\Delta_{nq}}{\mu_n \tanh \mu_n L} P_n. \tag{A.10}$$

Equations (A.7) and (A.10) can be combined in a linear system of equation as follows:

$$\begin{pmatrix} \left[\dfrac{L}{2}(1 + \delta_n)\right] & \left[\rho_f \omega^2 \displaystyle\sum_{q=0}^{\infty} \Delta_{nq}\right] \\ \left[b \displaystyle\sum_{n=0}^{\infty} \dfrac{\Delta_{nr}}{\mu_n \tanh \mu_n L}\right] & \left[(EI k_r^4 - \rho_s S \omega^2) \dfrac{L}{2}\right] \end{pmatrix} \begin{pmatrix} P_n \\ W_r \end{pmatrix} = \begin{pmatrix} 0 \\ \left[\dfrac{1 - (-1)^r}{k_r} f_{\text{ext}}\right] \end{pmatrix}. \tag{A.11}$$